Microstructure vs. Flaw: Mechanisms of Failure and Strength in Nanostructures.

ARTICLE *in* NANO LETTERS · OCTOBER 2013

Impact Factor: 13.59 · DOI: 10.1021/nl403453h · Source: PubMed

NANO LETTERS

Letter

pubs.acs.org/NanoLett

Microstructure versus Flaw: Mechanisms of Failure and Strength in Nanostructures

X. Wendy Gu,[†] Zhaoxuan Wu,[§] Yong-Wei Zhang,[§] David J. Srolovitz,[∥] and Julia R. Greer*[,‡]

[†]Division of Chemistry and Chemical Engineering, and [‡]Division of Engineering and Applied Science, California Institute of Technology, 1200 E. California Blvd., Pasadena, California 91125, United States

[§]Institute of High Performance Computing, 1 Fusionopolis Way, #16-16 Connexis, Singapore 138632, Singapore

[∥]Departments of Materials Science and Engineering & Mechanical Engineering and Applied Mechanics, University of Pennsylvania, Philadelphia, Pennsylvania 19104, United States

Supporting Information

ABSTRACT: Understanding failure in nanomaterials is critical for the design of reliable structural materials and small-scale devices with nanoscale components. No consensus exists on the effect of flaws on fracture at the nanoscale, but proposed theories include nanoscale flaw tolerance and maintaining macroscopic fracture relationships at the nanoscale with scarce experimental support. We explore fracture in nanomaterials using nanocrystalline Pt nanocylinders with prefabricated surface notches created using a "paused" electroplating method. In situ scanning electron microscopy (SEM) tension tests demonstrate that the majority of these samples failed at the notches, but that tensile failure strength is independent of whether failure occurred at or away from the flaw. Molecular dynamics simulations verify these findings and show that local plasticity is able to reduce stress concentration ahead of the notch to levels comparable with the strengths of microstructural features (e.g., grain boundaries). Thus, failure occurs at the stress concentration with the highest local stress whether this is at the notch or a microstructural feature.

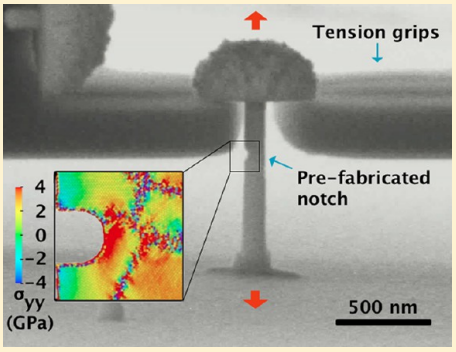

KEYWORDS: *Size effect, nanocrystalline, mechanical properties, fracture, molecular dynamics*

Hard biomaterials such as shell, bone, and exoskeletons have an exceedingly high strength and fracture toughness that are on par with the best manmade structural materials.[1,2] These biomaterials have a unifying feature; their internal structures are hierarchically arranged, with distinct features on length scales extending from the nano to the macro. Nanofabrication techniques have advanced to the point where it is now possible to emulate these hierarchical structures, for example, using ultrahigh strength nanoscale building blocks made of carbon and inorganic nanotubes (1D) and platelets (2D), and metals with nanoscale interfaces (3D) as the load-bearing components.[3−8] The high intrinsic strength of these nanomaterials is often difficult to maintain in large-scale composites because a macroscopic ensemble of these structures routinely contain structural and/or chemical features within individual constituents or at the interfaces, which are sources of failure initiation.[9,10] Classical fracture mechanics dictates that susceptibility to fracture depends on sample and/or external flaw length scales. This implies that different behavior may occur at small sample sizes and that new fracture relations may be necessary to describe the failure of nanoscale materials.[11,12]

Several theoretical and computational studies have been performed on fracture in preflawed nanoscale samples, often leading to conflicting interpretations. In the theoretical work of Gao et al., scaling arguments based on linear elastic fracture mechanics (LEFM) were used to define a critical length, 0.2−400 nm for typical brittle materials, below which the strength of a hard platelet becomes comparable to the theoretical strength of the material regardless of the presence of structural flaws.[13] These results were also supported by atomistic simulations on similar preflawed structures.[14] This nanoscale flaw tolerance, or flaw insensitivity, has been proposed as an explanation for the extraordinary toughness found in experiments on nanostructured biomaterials like nacre and spider silk[13,15] and in atomistic simulations of nanocrystalline aluminum thin films and polycrystalline graphene sheets, which showed failure occurring away from the prefabricated hole.[16,17] Other studies reported a strong dependence of failure on the presence of flaws—for example, in graphene and carbon nanotubes, where intentionally introduced holes led to strengths that are well below theoretical predictions, but in good agreement with predictions based upon classical fracture mechanics.[18] Even very small holes in carbon nanotube sidewalls consisting of 1−6 missing atoms were shown to reduce the nanotube strength by 26−33%.[19]

Few well-controlled experimental fracture tests have been attempted at the nanoscale. An in situ transmission electron

Received: September 16, 2013
Revised: October 17, 2013
Published: October 29, 2013

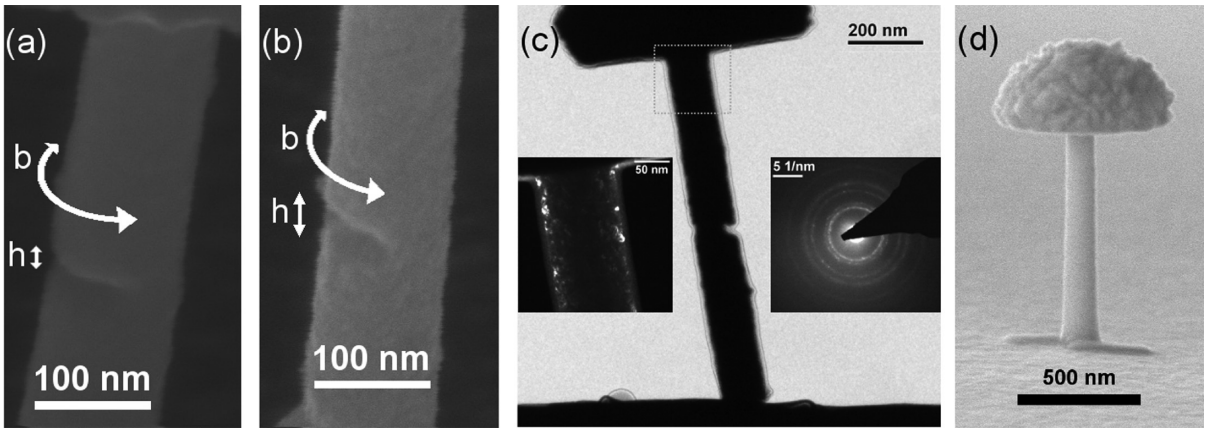

Figure 1. Nanocrystalline nanocylinders with intentionally introduced notches. SEM images taken from a 52° tilt of (a) a notch with circumferential length b = 84 nm and height h = 47 nm ($\overline{b}$ = 0.23 and $\overline{h}$ = 0.06 when normalized by sample dimensions) and (b) a notch of b = 161 nm and h = 24 nm ($\overline{b}$ = 0.54 and $\overline{h}$ = 0.03). (c) Bright-field TEM image of plucked cylinder, with the boxed region represented in the dark-field image inset which shows a nanocrystalline microstructure. The other inset shows the corresponding diffraction pattern. (d) SEM image of an unflawed cylinder.

microscopy (TEM) study of tensile-loaded nanocrystalline aluminum thin films, which contained focus ion beam (FIB) milled edge notches with a radius of ∼50 nm, showed that failure occurred far from the notch.[20] In other studies, traditional fracture testing methodologies were extended to micron-scale using FIB milled cantilever coupons (1−10 μm in size) to investigate failure in single and bicrystalline metals and alloys.[21−23] Results demonstrate that these micron-sized metals fractured as predicted by LEFM, with fracture strength and location controlled by the FIB-milled structural flaw.

These studies prompt several important questions about fracture at the nanoscale, including (1) does fracture strength depend on the presence of flaws and on sample/flaw geometry? and (2) can the initiation point of the crack that leads to failure be predicted based upon the location of the flaw? We address these questions by conducting tensile fracture experiments and molecular dynamics (MD) simulations on similar nanosized samples with introduced surface flaws of known geometries. In this work, the term "flaw" refers to the external notches only. Nanocrystalline Pt, referred to as nc-Pt hereafter, nanocylinders with surface notches were fabricated through pulsed electroplating into poly(methyl methacrylate) (PMMA) templates and do not suffer from FIB-induced damage common to many nanomechanical experiments. Typical Pt samples were ∼120 nm in diameter with an ∼6 nm grain size. Tensile experiments on unnotched nc-Pt nanocylinders revealed brittle failure, rendering this to be an appropriate material model system for testing fracture mechanics theories that assume limited plasticity. Sizes of surface notches in these nanostructures were of the same order of magnitude as internal microstructural features, that is, grain size. We examine the competition between such prefabricated flaws and intrinsic microstructural features as preferred sites for crack initiation and discuss these findings using concepts from LEFM and atomistic simulations.

Nanocrystalline platinum cylinders with diameters of 117 ± 3 nm and lengths of 750 ± 40 nm were fabricated with one or more surface flaws using a template-assisted electroplating method described in Gu et al.[24] Cylinders were electroplated into nanoscale pores in PMMA on top of a conductive gold surface. The PMMA layer was subsequently removed to leave freestanding cylinders. Nanoscale structural flaws were formed on the outer surface of the cylinder by ramping voltage from 0 to 0.6 V at 85 mV/s, pausing the electroplating process for approximately five minutes, replacing the electroplating bath, and then applying two more pulses at the same voltage and plating rate. Applying three electroplating pulses was appropriate for filling the PMMA pore and forming a hemispherical "head" above the PMMA layer that can subsequently be used as a grip during tension testing. We postulate that this fabrication technique leads to surface flaws because the first electroplating pulse leads to the formation of a columnar cylinder with several grains exposed on the top surface of the cylinder. The second set of pulses leads to the nucleation of new grains at some but not all of the exposed grains on the top surface of some of the cylinders. The flaw is formed where nucleation fails to occur between sets of electroplating pulses.

The surface flaws had the shape of a rounded notch with circumferential length, b, and height, h (see Figure 1a and b). The geometry of each cylinder and its surface flaws was characterized thoroughly using scanning electron microscopy (SEM) at a 52° tilt at 0° (to image the front face of the cylinder) and 180° (back face) rotation and at 86° tilt at 0° rotation (front face). The notch depth, a, and radius, r, were estimated using this method but could not be determined precisely because SEM imaging cannot be performed at the necessary angles relative to the notch for complete characterization of a and r. Notch geometries were grouped into two categories: (1) a straight notch or (2) a partial circumferential notch based on SEM images, with r equal to half of h (see Supporting Information, Figure S1). Notch geometry was described in terms of the fraction of cylinder circumference, $\overline{b} = b/\pi D$, and fraction of the cylinder height, $\overline{h} = h/l$. Resulting unitless dimensions were $\overline{b}$ = 0.10−0.50 (circumferential length of b = 40−200 nm) and $\overline{h}$ = 0.02−0.07 (notch height h = 15−50 nm) (Figure 1).

The size and shape of nanoscale samples and flaws play an important role in failure processes; hence to compare fracture properties in a nanomaterial with those with macroscopic dimensions, it would be wise to follow a standard for nanomechanical testing. Existing ASTM fracture standards are designed for large samples, and no standard exists for nanoscale samples.[25] This work serves as a step toward establishing this standard because it sheds light on fundamental physics of fracture mechanisms in nanomaterials in the presence of notches, which play a key role in failure of macroscopic

dx.doi.org/10.1021/nl403453h | Nano Lett. 2013, 13, 5703−5709

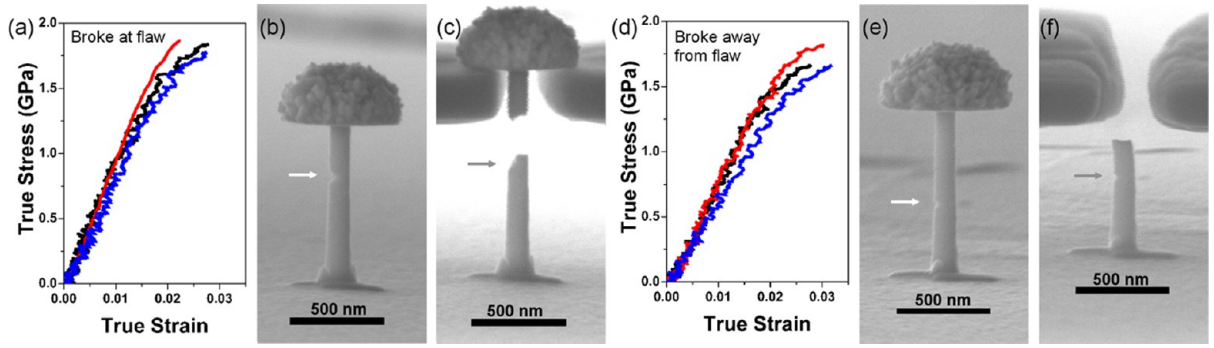

Figure 2. Samples that broke at the flaw: (a) representative true stress–true strain plots from uniaxial tension tests, (b) SEM image of a preflawed sample, and (c) SEM image of the same sample after fracturing at the flaw. Samples that broke away from the flaw: (d) representative true stress–true strain plots from uniaxial tensile tests, (e) SEM image of a preflawed sample, and (f) SEM image of the same sample after fracturing away from the flaw.

samples. The sample geometry in this work is appropriate for nanofracture testing because the surface flaws represent a major stress concentrator at which failure initiation would be expected in a typical macroscopic sample. The nc-Pt samples failed at ~3% strain and approximately 1% plastic strain with no observable bending at the flaw.

Sample preparation for TEM was performed by "plucking" a tension sample with the InSEM (Nanomechanics, Inc.), an in situ SEM with an attached nanoindenter.[26] To do this, the tension sample was fed into a custom-milled tungsten tension grip used as the nanoindenter tip, which is used to lift the sample off the growth substrate. The grips were in contact with the sample on the underside of the tension head. The sample was then gently lowered onto a TEM grid using the tension grips, and then the tension grip was detached from the tension head. Carbon is applied to the base of the sample using e-beam deposition to glue the sample to the TEM grid. TEM revealed the grain size to be 6 ± 3 nm with no significant variation across sample volumes.

Tension tests were performed in the InSEM using a custom-milled diamond tension grip.[27] Electroplated Pt cylinders show poor adhesion to the underlying Au substrate, so a small amount of W glue was applied to the base of the cylinder using the FEI Nova 200 dual beam system. Tension tests were conducted at a constant strain rate of 0.01 s^{-1}. SEM video was taken during tension testing, and instrument compliances, changes in sample dimensions, and fracture locations were determined from the video. Measured load–displacement data was converted to true stress–strain curves, after accounting for instrument compliance. During in situ SEM mechanical tests the samples were oriented such that the surface flaw was on the side, rather than the front or back faces, of the sample relative to the imaging electron beam to observe the initiation of failure (see Figure 2). We found that 8 of 12 samples broke at the surface flaw, and the remaining 4 broke away from the flaw (see SI for in situ SEM movies). Stress–strain data for each experiment suggested brittle failure, with limited plastic deformation and no noticeable necking (Figure 2a,d). The data showed no significant difference in ultimate tensile strengths (UTS) of samples that broke at the flaw (UTS of 1.8 ± 0.1 GPa), ones that broke away from the flaw (UTS of 1.8 ± 0.2 GPa), and the unnotched samples. This strength is 50% higher than that of similarly fabricated Pt nanopillars tested in compression, which is likely due to the higher deformation strain rate (0.001 s^{-1} for compression vs 0.01 s^{-1} here) and the tension–compression asymmetry common to nanocrystalline metals.[24,28] Sample size-dependent weakening appears in nanocrystalline Pt nanostructure when the sample size to grain size ratio, D/d, falls below ~5.[24] Samples in this study have a D/d of ~20; hence, the measured strengths are independent of sample size.

Finite element modeling (FEM) was used to estimate the stress concentration due to the external flaw on 11 of the 12 experimentally tested nanocylinders to evaluate whether failure location and strength correlate with stress concentration at the notch. The calculations showed that the stress concentrations at the notches in the cylinders that broke at the notch to be higher than those for notched samples that broke elsewhere for all but one sample. FEM simulations also revealed that elasticity-based stress concentrations were not correlated with the experimental UTS (see SI text, Figures S2–S4).

SEM images revealed features with dimensions on the order of grain size that populated the fracture surfaces, reminiscent of typical dimpled fracture morphology of bulk nanocrystalline metals[29,30] (see SI text, Figure S5). This suggests the occurrence of localized plasticity despite no evidence of global necking. The angle between the fracture surface relative to the loading axis and the curvature of the fracture surface across the width of the broken cylinder varied among the samples.

The finding that 2/3 of the samples broke at the notch suggests sensitivity of failure initiation to flaws. Both sets of cylinders—ones that failed at the flaw and those that failed away from it—exhibited nearly identical fracture strengths, which implies flaw insensitivity in strength. To resolve this apparent contradiction, we performed molecular dynamics simulations of nc-Pt samples with notch and sample geometries similar to those in the experiments to reveal the mechanistic origin of the experimentally observed deformation and failure.

A periodic simulation cell (64 × 206 × 64 nm) was created in which 648 "seeds" were randomly placed, and upon which Voronoi tessellations are performed. The resulting Voronoi polyhedra were then filled with atoms in a perfect face-centered cubic Pt crystal of random orientation to produce a nanocrystalline structure with an average grain size of ~14 nm. Nanocrystalline Pt nanocylinders of diameter ~43 nm and a film of thickness ~20 nm were carved from this periodic bulk nanostructure. MD simulations were performed using the Large-scale Atomic/Molecular Massively Parallel Simulator (LAMMPS), where interactions between Pt atoms were described using the Embedded Atom Method (EAM) potential parametrized by Sheng et al.[31–33] Periodic boundary conditions were imposed along the nanocylinder axes and lengthwise along

dx.doi.org/10.1021/nl403453h | Nano Lett. 2013, 13, 5703–5709

the film, while other surfaces were free. All of the structures were equilibrated at 300 K before tensile loading was applied.[34] Uniaxial tensile loading was applied at a constant true strain rate of 0.1 ns^{-1}. During tensile loading, constant temperature was maintained using a Nosé–Hoover thermostat.[35−38] The atomic stresses were calculated based on the atomic *virial* stress in which the atomic volume was set to the Voronoi volume associated with each atom.

A notch-free nanocylinder (Figure 3a) was created and used as the starting structure for four nanocylinder samples with

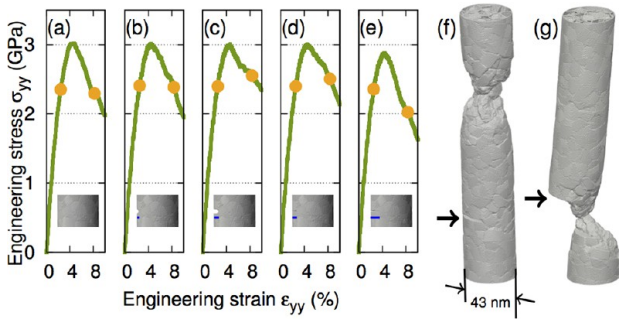

Figure 3. Stress–strain curves of 5 simulation samples for (a) notch-free and notched samples with notch geometry with normalized circumferential width and height (b) $\bar{b}$ = 0.16 and $\bar{h}$ = 0.03 (b = 21 nm and h = 5 nm), (c) $\bar{b}$ = 0.2 and $\bar{h}$ = 0.03 (b = 30 nm and h = 5 nm), (d) $\bar{b}$ = 0.23 and $\bar{h}$ = 0.006 (b = 31 nm and h = 1 nm), and (e) $\bar{b}$ = 0.33 and $\bar{h}$ = 0.006 (b = 44 nm and h = 1 nm). In the stress–strain curves, the orange circles mark the 2.5% and 8% strains at which the atomic stresses in Figure 2 were measured. The insets in a–e show magnified views near the notches, and the blue lines indicate the notch depths. (f–g) Examples of pillar fracture away from the notch ($\bar{b}$ = 0.23; $\bar{h}$ = 0.006) and at the notch ($\bar{b}$ = 0.33 and $\bar{h}$ = 0.006), respectively.

notches of very different geometries. Two samples had rounded notches ($\bar{b}$ = 0.16 and $\bar{h}$ = 0.03, Figure 3b; $\bar{b}$ = 0.2 and $\bar{h}$ = 0.03, Figure 3c), and two samples contained sharp notches ($\bar{b}$ = 0.23 and $\bar{h}$ = 0.006, Figure 3d; $\bar{b}$ = 0.33 and $\bar{h}$ = 0.006, Figure 3e). Following equilibration at room temperature, the nanocylinders were uniaxially stretched to failure.[34] Before creating the notch, we first identified the fracture location in the notch-free nanocylinder and always placed the notches far away from this location.

Figure 3 shows the stress–strain data for all five nanocylinders (a–e) and post-deformation samples that break away from (f) and at (g) the notch. Simulations revealed that the samples shown in Figure 3b and d broke away from the notch, in contrast to those in Figure 3c and e, which failed at the notch. Regardless of the location of failure initiation, all stress–strain curves were remarkably similar, reaching a UTS of ∼3 GPa, and then undergoing rapid strain softening even in the most extreme case in which the notch extended 1/3 across the sample diameter (Figure 3e). The nearly identical UTS in all five samples demonstrates that the UTS was insensitive to the presence of notches, and the occurrence of failure both at and away from the notches suggests sensitivity of failure initiation to flaws, which corroborates the experiments.

These experimental and computational results present compelling evidence that the effects of flaws on deformation and failure of nanomaterials are significantly different from those in their coarse-grained and macroscopic counterparts. To gain further insight into what makes failure of nanomaterials different in response to external notches, we examined these processes at the atomic level. Figure 4 shows the spatial

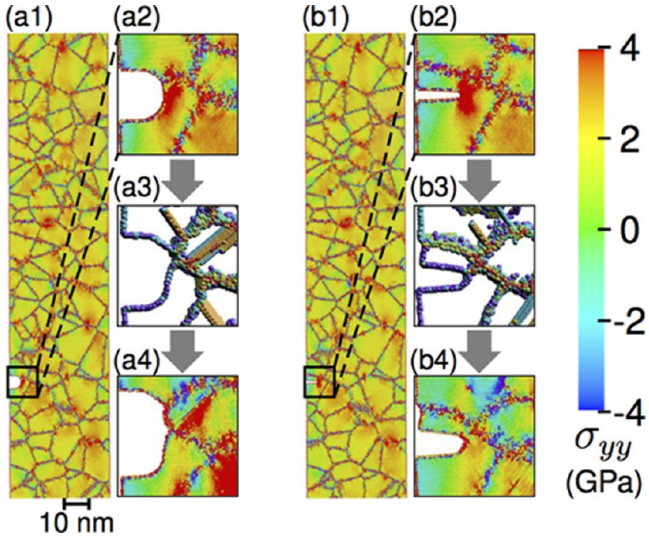

Figure 4. (a1–a2) Cross-sectional view of tensile stress (σ_{yy}) at 2.5% applied strain in simulated samples with rounded notch geometry ($\bar{b}$ = 0.2 and $\bar{h}$ = 0.03), and sharper notch geometry ($\bar{b}$ = 0.23 and $\bar{h}$ = 0.006). (a2–b2) Magnification at notch showing stress concentration at notch tip. (a3–b3) Notch blunting by dislocation and grain boundary plasticity at 6.5% applied strain. (a4–b4) Stress contours show absence of stress concentrations near notches at 8% strain because of previously active plasticity mechanisms. In a3–b3, atoms are shown only if their central symmetry parameters differ from that of the perfect FCC crystal; the colors indicate the local symmetry.[39] Atoms on twin boundaries, dislocations, and intrinsic and extrinsic stacking faults are shown in light blue, dark blue or green (depending on dislocation type), orange, and light blue, respectively.

distribution of atomic-level (virial) tensile stresses (σ_{yy}) near a rounded notch ($\bar{b}$ = 0.2 and $\bar{h}$ = 0.03) and near a sharp notch ($\bar{b}$ = 0.23 and $\bar{h}$ = 0.006) at a 2.5% applied strain. The stress distribution near both type of notches showed the presence of a strong stress concentration at the tip of the notch, which is ∼5 times the average stress (a2–b2), and is sufficiently large to trigger highly localized plasticity at the notch. Partial dislocations were nucleated at the rounded notch root and propagated across the grain, leaving stacking faults in their wake (Figure 4a3). Grain boundary sliding occurred in response to the local stress at the sharper notch, which led to surface offsets where grain boundaries intersected the outer surface (Figure 4b3, see SI for movies of stress evolution during fracture). The combination of grain boundary sliding and partial dislocation nucleation and propagation represents the intrinsic deformation mechanism of nanocrystalline Pt nanostructures.[24] Grain boundary sliding generally occurs at a lower applied stress than does dislocation nucleation but also depends on other factors such as the presence of neighboring grains with favorable orientations and proximity to free surfaces. Thus, the specific plasticity mechanism active at the notch cannot be predicted from notch geometry alone, although notch geometry influences the local stress.

Surprisingly, the plastic activity near the notches was found to be sufficient to reduce the local stress almost to the background stress level as shown in Figure 4a4–b4. These notches no longer served as "hot spots" with regard to elevated local stress. The notch roots became blunted, thereby shielding

dx.doi.org/10.1021/nl403453h | *Nano Lett.* 2013, 13, 5703–5709

the material near the notch from further stress increase. Subsequent localized plasticity in the samples occurred at other stress concentrators in the sample, such as grain boundary triple junctions. This analysis shows that even a severe notch with a strong initial stress concentration may not dominate failure in a sample because plasticity mechanisms inherent to the nanocrystalline material can render the notch ineffective as a stress concentration at later stages of deformation.

Figure 5 presents a compelling example of localized plasticity at the notch, which reduces the stress concentration by blunting

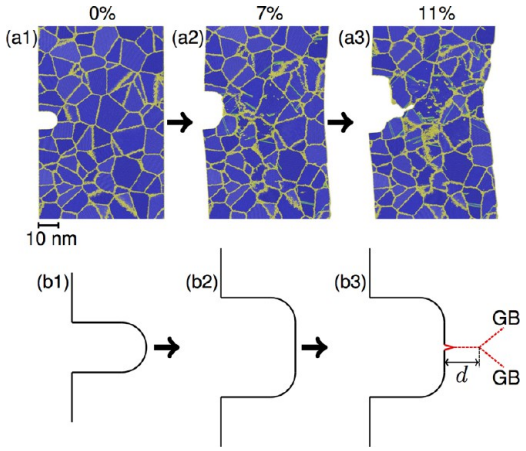

Figure 5. Cross-sectional view of intergranular fracture at the notch tip in a Pt polycrystalline film. (a1) Notch at 0% strain, (a2) at 7% strain where the notch is blunted by local plasticity emanates from the notch tip, and (a3) 11% strain where intergranular fracture initiates at the notch. Atoms are colored based on their structural type as determined by common neighbor analysis: blue for atoms at lattice positions, green for atoms at stacking faults, and yellow for atoms at grain boundaries.[40] (b1–b3) The corresponding schematics showing the undeformed notch geometry, notch blunting, and widening and intergranular fracture occurring at a grain boundary with characteristic size d.

and exposes the intrinsic failure mechanism. Figure 5a1 shows an undeformed nanocrystalline slab geometry sample. Figure 5a2 shows the same sample under an applied load, in which the emission of dislocations and grain boundary sliding led to large localized deformation at the notch and significant blunting. In Figure 5a3, a crack formed along a grain boundary at the notch root and propagated unstably, which ultimately led to failure. Schematic illustrations (Figure 5b1–b3) of the change in notch geometry during the deformation process show the process of an initial, rounded notch elongating and blunting under tension and finally fracturing along a grain boundary by the formation of a crack-like defect with characteristic size equal to the grain size, d. The same failure mechanism can also lead to failure away from the notch and applies to the deformation and failure in the unnotched samples. This is because a crack-like defect can also form at an internal grain boundary (where the stress cannot be further relaxed due to the small crack size), which causes the adjacent grains to pull apart under tension (see SI text, Figure S6). The intrinsic failure strength of such a crack-like defect can be estimated using the Griffith equation, $\sigma_f = \sqrt{E\gamma\rho/4ar_0}$, in which E, γ, ρ, a, and r_0 are the elastic modulus, surface energy, crack radius, crack length, and interatomic spacing, respectively. We assume that $\rho = r_0$ for a sharp crack and $a \approx d$, where d is the grain size. Using E = 160 GPa and γ = 2 J/m^2, we estimate the Griffith fracture strength to be 3 GPa.[33] This is within a factor of 2 of the measured fracture strength from experiments and simulations with no adjustable parameters. While Griffith theory applies only to brittle materials, it is reasonable to use in the nanocrystalline samples studied here because no dislocations are generated near the grain-sized crack (which is much smaller than the external notch) to plastically relax the crack stress field and dissipate energy.

The fundamental picture of failure in nanocrystalline nanostructures with surface flaws that emerges from experiments and simulations is that the competition between stress concentrators due to external flaws and intrinsic microstructural features governs failure strength and location. The samples studied here contain a statistical distribution of internal stress concentrators associated with the microstructure, as well as an external stress concentration in the form of the notch. The dominant internal stress concentrators in these nanocrystalline samples are grain boundary triple junctions. Such features are ubiquitous within nanocrystalline samples with the sample diameter large compared to the grain size. The strength of triple junctions as stress concentrators depends on the orientation of the sliding grain boundaries relative to the load as well as on the orientation of the slip systems within the grains for dislocation nucleation. This gives rise to a statistical distribution of stress concentrators associated with microstructural features. As the sample is loaded in tension, the internal or external feature with the highest stress concentration is activated and reaches a local stress at which it either relaxes plastically or breaks. If relaxation occurs at this site, this sequence of events repeats at the site of the next highest stress concentration. This process continues to cascade until the active site cannot relax, and fracture ensues.

Samples tend to fail at the external flaw because the surface notch is generally the site with either the highest or one of the highest initial stress concentrations. In samples where failure occurred at the flaw, the failure criteria was first met at the external notch, prior to any plasticity mechanism reducing the local stress at the external flaw to the level of the next weakest site. Grain boundary sliding occurs more easily at the flaw because of the initially high local stress at this location, which means that the intrinsic failure mechanism is more likely to operate at this location rather than elsewhere in the sample.

A direct consequence of such a failure mechanism is flaw insensitivity in strength because the same intrinsic failure mechanism leads to failure, regardless of whether failure occurs at or away from the notch. Since the fundamental failure mechanisms are the same in the presence or absence of notches, the UTS is insensitive to exactly where the failure process starts. The cascade of stress relaxation at stress concentrators via localized plastic deformation dictates that the stress concentration at these locations reaches similar levels, which gives rise to the narrow range of UTS measured in experiment and simulation. This phenomenon is unique to nanocrystalline, nanoscale solids because large stress concentrations can be plastically relaxed (via localized deformation), but those associated with the nanoscale microstructure features cannot be relaxed because they are too small for dislocation nucleation (and localized plasticity). In a macroscale nanocrystalline system, the UTS can be modulated by introduction of very large, sharp flaws that create plastic zones that are too large to be relaxed by local plastic deformation. In such cases, the ultimate failure mode is likely to be more ductile than in our experiments on nanosamples, which show brittle fracture.

dx.doi.org/10.1021/nl403453h | Nano Lett. 2013, 13, 5703–5709

Although the MD simulations demonstrate excellent qualitative agreements with experimental results, quantitative differences exist. MD simulations show a moderately ductile fracture on the scale of the grain size, while the experiments suggest a "brittle" fracture process. This discrepancy could be attributed to the differences in grain sizes (6 nm in experiments vs 14 nm in simulations), the number and orientation of the grains across the cylinder diameter and ahead of notches, and from the much higher strain rates in the simulations. Nevertheless, the experiments and simulations unambiguously demonstrate that failure initiation in nanomaterials is determined by intrinsic microstructural failure mechanisms and that the UTS is insensitive to the presence of notches.

The results presented here can be summarized as: (1) flaw *insensitivity* in strength: strength does not depend on whether failure initiates at an external flaw or within the microstructure, and (2) flaw *sensitivity* in fracture location: most nc-Pt nanocylinders broke at the prefabricated flaws regardless of fracture strength as long as the flaw was sufficiently large/sharp. These observations can be explained through competition between internal microstructural features and the external flaw. Brittle failure occurs at a constant stress, independent of the notch provided that the stress-field at the notch is small enough that ductile fracture does not occur and that the microstructural features (crack nucleation sites) are too small to emit dislocations (plastically relax). In classes of materials where plastic deformation cannot occur easily (e.g., ceramics), local plastic relaxation at the notch tip may not be possible, and hence such nanomaterials may still fail at a notch-dependent ultimate stress. In the case of nanocrystalline Pt nanostructures, nucleating dislocations is fairly easy; in other nanomaterials, it is possible that non-dislocation plasticity could play a similar role—for example, polymer flow between ceramic units, as in many strong and tough biological materials.

The competition between stress concentrations within the sample naturally leads to flaw sensitivity in failure initiation location, because incipient deformation and subsequent failure occur at the position of the stress concentration which first satisfies the failure criteria. The localized plasticity in the vicinity of stress concentrators, that is, triple junctions or flaws, tends to reduce the initially present stress concentrations, which leads to a more effective competition of the multiple stress concentrators throughout the sample volume. This process results in similar fracture strengths for a wide range of flaw shapes and sizes, which is manifested as flaw insensitivity in strength.

Major external flaws do not necessarily reduce the strength of nanoscale and nanostructured materials yet may still serve as sites of failure initiation if the intrinsic failure criterion is reached because of the high local stress compared to stresses at internal, microstructural features. The high strength intrinsic to many nanostructures can be maintained while increasing fracture toughness, or resistance to failure at flaws, through microstructural toughening mechanisms. These findings shed light on failure processes in nanomaterials, which commonly show significant deviations from mechanical behavior expected from classical continuum theory. Microstructure and external size information must also be included when predicting failure in nanomaterials. The present results suggest that future nanofracture testing be performed with careful consideration of microstructural effects as well as well-defined and characterized sample and notch geometries. Sample and notch geometries appropriate for application of classical continuum theories may not be accessible in nanostructures where internal, microstructural features also have an important influence on failure.

■ ASSOCIATED CONTENT

Ⓢ Supporting Information

Modeling of notch geometry, finite element modeling of notched cylinders, fracture surface morphology, and crack formation at internal grain boundary, plus molecular dynamics and in situ SEM movies. This material is available free of charge via the Internet at http://pubs.acs.org.

■ AUTHOR INFORMATION

Corresponding Author

*Phone: 626-395-4127; e-mail: jrgreer@caltech.edu.

Notes

The authors declare no competing financial interest.

■ ACKNOWLEDGMENTS

X.W.G. is grateful for financial support from the National Defense Science and Engineering Graduate (NDSEG) Fellowship, 32 CFR 168a. J.R.G. acknowledges the financial support of the National Science Foundation (DMR-1204864). X.W.G. and J.R.G. thank the Kavli Nanoscience Institute at Caltech for the availability of critical cleanroom facilities. We thank V. Deshpande and D. Jang for helpful discussion and D. Jang and C. Garland for TEM assistance. The authors gratefully acknowledge the financial support from the Agency for Science, Technology and Research (A*STAR), Singapore and the use of computing resources at the A*STAR Computational Resource Centre, Singapore.

■ REFERENCES

(1) Currey, J. D. Mechanical-Properties of Mother of Pearl in Tension. *Proc. R. Soc. B: Biol. Sci.* **1977**, *196*, 443−463.

(2) Fratzl, P.; Weinkamer, R. Nature's hierarchical materials. *Prog. Mater. Sci.* **2007**, *52*, 1263−1334.

(3) Yu, M. F.; Lourie, O.; Dyer, M. J.; Moloni, K.; Kelly, T. F.; Ruoff, R. S. Strength and breaking mechanism of multiwalled carbon nanotubes under tensile load. *Science* **2000**, *287*, 637−640.

(4) Lee, C.; Wei, X. D.; Kysar, J. W.; Hone, J. Measurement of the elastic properties and intrinsic strength of monolayer graphene. *Science* **2008**, *321*, 385−388.

(5) Garel, J.; Leven, I.; Zhi, C. Y.; Nagapriya, K. S.; Popovitz-Biro, R.; Golberg, D.; Bando, Y.; Hod, O.; Joselevich, E. Ultrahigh Torsional Stiffness and Strength of Boron Nitride Nanotubes. *Nano Lett.* **2012**, *12*, 6347−6352.

(6) Bertolazzi, S.; Brivio, J.; Kis, A. Stretching and Breaking of Ultrathin MoS_2. *ACS Nano* **2011**, *5*, 9703−9709.

(7) Lu, L.; Chen, X.; Huang, X.; Lu, K. Revealing the Maximum Strength in Nanotwinned Copper. *Science* **2009**, *323*, 607−610.

(8) Uchic, M. D.; Dimiduk, D. M.; Florando, J. N.; Nix, W. D. Sample dimensions influence strength and crystal plasticity. *Science* **2004**, *305*, 986−989.

(9) Vigolo, B.; et al. Macroscopic fibers and ribbons of oriented carbon nanotubes. *Science* **2000**, *290*, 1331−1334.

(10) Hao, S.; et al. A transforming metal nanocomposite with large elastic strain, low modulus, and high strength. *Science (New York, N.Y.)* **2013**, *339*, 1191−1194.

(11) Dugdale, D. S. Yielding of Steel Sheets Containing Slits. *J. Mech. Phys. Solids* **1960**, *8*, 100−104.

(12) Hertzberg, R. W. *Deformation and Fracture Mechanics of Engineering Materials*; Wiley: New York, 1995.

(13) Gao, H. J.; Ji, B. H.; Jager, I. L.; Arzt, E.; Fratzl, P. Materials become insensitive to flaws at nanoscale: Lessons from nature. *Proc. Natl. Acad. Sci. U.S.A.* **2003**, *100*, 5597−5600.

(14) Buehler, M. J.; Yao, H. M.; Gao, H. J.; Ji, B. H. Cracking and adhesion at small scales: atomistic and continuum studies of flaw tolerant nanostructures. *Modell. Simul. Mater. Sci. Eng.* **2006**, *14*, 799−816.
(15) Giesa, T.; Pugno, N. M.; Buehler, M. J. Natural stiffening increases flaw tolerance of biological fibers. *Phys. Rev. E* **2012**, *86*, 041902.
(16) Kumar, S.; Li, X. Y.; Haque, A.; Gao, H. J. Is Stress Concentration Relevant for Nanocrystalline Metals? *Nano Lett.* **2011**, *11*, 2510−2516.
(17) Zhang, T.; Li, X. Y.; Kadkhodaei, S.; Gao, H. J. Flaw Insensitive Fracture in Nanocrystalline Graphene. *Nano Lett.* **2012**, *12*, 4605−4610.
(18) Khare, R. M.; Mielke, S. L.; Paci, J. T.; Zhang, S. L.; Ballarini, R.; Schatz, G. C.; Belytschko, T. Coupled quantum mechanical/molecular mechanical modeling of the fracture of defective carbon nanotubes and graphene sheets. *Phys. Rev. B* **2007**, *75*, 075412.
(19) Mielke, S. L.; et al. The role of vacancy defects and holes in the fracture of carbon nanotubes. *Chem. Phys. Lett.* **2004**, *390*, 413−420.
(20) Kumar, S.; Haque, M. A.; Gao, H. Notch insensitive fracture in nanoscale thin films. *Appl. Phys. Lett.* **2009**, *94*, 253104.
(21) Wurster, S.; Motz, C.; Pippan, R. Characterization of the fracture toughness of micro-sized tungsten single crystal notched specimens. *Philos. Mag.* **2012**, *92*, 1803−1825.
(22) Iqbal, F.; Ast, J.; Goken, M.; Durst, K. In situ micro-cantilever tests to study fracture properties of NiAl single crystals. *Acta Mater.* **2012**, *60*, 1193−1200.
(23) Kupka, D.; Lilleodden, E. T. Mechanical Testing of Solid-Solid Interfaces at the Microscale. *Exp. Mechanics* **2012**, *52*, 649−658.
(24) Gu, X. W.; Loynachan, C. N.; Wu, Z. X.; Zhang, Y. W.; Srolovitz, D. J.; Greer, J. R. Size-Dependent Deformation of Nanocrystalline Pt Nanopillars. *Nano Lett.* **2012**, *12*, 6385−6392.
(25) Wilson, C. D.; Landes, J. D. *Fracture toughness testing with notched round bars*; ASTM STP 1360; ASTM: West Conshohocken, PA, 2000; Vol. *30*, ID STP13396S.
(26) Jang, D.; Li, X.; Gao, H.; Greer, J. R. Deformation mechanisms in nanotwinned metal nanopillars. *Nat. Nanotechnol.* **2012**, *7*, 594−601.
(27) Kim, J. Y.; Jang, D. C.; Greer, J. R. Insight into the deformation behavior of niobium single crystals under uniaxial compression and tension at the nanoscale. *Scr. Mater.* **2009**, *61*, 300−303.
(28) Jang, D. C.; Greer, J. R. Size-induced weakening and grain boundary-assisted deformation in 60 nm grained Ni nanopillars. *Scr. Mater.* **2011**, *64*, 77−80.
(29) Dalla Torre, F.; Van Swygenhoven, H.; Victoria, M. Nanocrystalline electrodeposited Ni: microstructure and tensile properties. *Acta Mater.* **2002**, *50*, 3957−3970.
(30) Hasnaoui, A.; Van Swygenhoven, H.; Derlet, P. M. Dimples on nanocrystalline fracture surfaces as evidence for shear plane formation. *Science* **2003**, *300*, 1550−1552.
(31) Plimpton, S. Fast Parallel Algorithms for Short-Range Molecular-Dynamics. *J. Comput. Phys.* **1995**, *117*, 1−19.
(32) Daw, M. S.; Baskes, M. I. Embedded-Atom Method - Derivation and Application to Impurities, Surfaces, and Other Defects in Metals. *Phys. Rev. B* **1984**, *29*, 6443−6453.
(33) Sheng, H. W.; Kramer, M. J.; Cadien, A.; Fujita, T.; Chen, M. W. Highly optimized embedded-atom-method potentials for fourteen fcc metals. *Phys. Rev. B* **2011**, *83*, 134118.
(34) Wu, Z. X.; Zhang, Y. W.; Jhon, M. H.; Gao, H. J.; Srolovitz, D. J. Nanowire Failure: Long = Brittle and Short = Ductile. *Nano Lett.* **2012**, *12*, 910−914.
(35) Nose, S. A Unified Formulation of the Constant Temperature Molecular-Dynamics Methods. *J. Chem. Phys.* **1984**, *81*, 511−519.
(36) Nose, S. A Molecular-Dynamics Method for Simulations in the Canonical Ensemble. *Mol. Phys.* **1984**, *52*, 255−268.
(37) Hoover, W. G. Constant-Pressure Equations of Motion. *Phys. Rev. A* **1986**, *34*, 2499−2500.
(38) Melchionna, S.; Ciccotti, G.; Holian, B. L. Hoover NPT Dynamics for Systems Varying in Shape and Size. *Mol. Phys.* **1993**, *78*, 533−544.
(39) Kelchner, C. L.; Plimpton, S. J.; Hamilton, J. C. Dislocation nucleation and defect structure during surface indentation. *Phys. Rev. B* **1998**, *58*, 11085−11088.
(40) Faken, D.; Jonsson, H. Systematic analysis of local atomic structure combined with 3D computer graphics. *Comput. Mater. Sci.* **1994**, *2*, 279−286.